ENVIRONMENTAL RESEARCH
LETTERS

OPEN ACCESS

RECEIVED
11 April 2025

REVISED
29 May 2025

ACCEPTED FOR PUBLICATION
16 June 2025

PUBLISHED
1 July 2025

LETTER

The winter North Atlantic Oscillation downstream teleconnection: insights from large-ensemble climate model simulations

Sing Lau, Kunhui Ye* and Tim Woollings

Atmospheric, Oceanic, & Planetary Physics, University of Oxford, OX1 3PU Oxford, United Kingdom
* Author to whom any correspondence should be addressed.

E-mail: kunhui.ye@physics.ox.ac.uk

Keywords: North Atlantic Oscillation (NAO), teleconnection, downstream climate predictability, CMIP6, large-ensemble climate model simulations, internal climate variability, Rossby waveguides

Abstract

The winter North Atlantic Oscillation (NAO) is the dominant pattern of atmospheric circulation variability over the North Atlantic region. It influences climate and weather such as surface air temperatures downstream over Eurasia through establishing a large-scale teleconnection, but past studies on the NAO's downstream teleconnection have been largely limited to observational data, and further evidence of downstream impacts and associated mechanisms from comprehensive climate modeling is desirable. This study quantifies and analyzes this teleconnection on an interannual timescale by using both ERA5 reanalysis, and five large ensembles from four climate simulation models. A particular focus is placed on dynamical pathways, as well as variability among ensemble members that modulates the teleconnection strength. Results suggest that NAO signals are propagated downstream by Rossby waves, efficiently transmitted through waveguides along *both* the polar and subtropical jet streams to Eastern Eurasia; while heat can be advected weakly from upstream, advection plays a rather local effect inducing temperature anomalies from the Pacific Ocean onshore. Multiple linear regression shows that internal climate variability significantly modulates the teleconnection: a more locally dominant NAO pattern, and narrower waveguides could strengthen the teleconnection. These two factors combine to explain up to 70% of variance in the teleconnection strength, with each contributing almost equally. Reanalysis data marginally agree with the regression model (1.9 standardized residuals higher in strength), suggesting potential model biases in jets and the NAO variability. Monitoring these modulating factors would be crucial to understanding downstream climate predictability and improving climate prediction models linked to the NAO.

1. Introduction

The North Atlantic Oscillation (NAO) is the dominant fluctuation pattern of sea level pressure (SLP) over the North Atlantic region. While focused on the North Atlantic, the teleconnection exerts an influence over much of the hemisphere with impacts on temperature and precipitation (Hurrell and Van Loon 1997, Branstator 2002, Luo *et al* 2015, Ye *et al* 2022). The representation of the NAO itself in reanalysis and climate simulation models has been extensively examined, with many studies evaluating model skill in capturing its spatial pattern and temporal variability (Lee *et al* 2021, Baker *et al* 2024). These evaluations generally show decent correspondence between reanalysis and model outputs, providing a basis for assessing its downstream impacts. Specifically, the NAO is known to impact surface air temperatures (SATs) downstream of Europe, with a notable belt of high temperature correlation downstream extending to Northeast Asia (Hurrell 1996, Schlichtholz 2019). Ye *et al* (2022) showed that a large-scale mode of variability over the North Atlantic-Eurasian sector dominated by the NAO drives climate variability in the region, suggesting prominent downstream teleconnection of the NAO. This study focuses on the NAO between December and February (DJF) on an interannual timescale. The

predictability and wide influence of the winter NAO could make it a good predictor of climate and weather beyond the Atlantic region.

There have been a range of studies which investigate the dynamics and pathways of the downstream teleconnection. Xie *et al* (1999) suggested that advection from upstream winds and mean westerlies works as a mechanism to bring anomalous temperatures to downstream regions. Watanabe (2004) showed that stationary Rossby waves could transmit NAO signals along the subtropical (Asian) jet, with a waveguiding mechanism that directs the waves downstream, bringing geopotential anomalies to remote regions. Using wave activity fluxes (WAFs), Song *et al* (2014) presented two possible wave transmission pathways along the polar and subtropical jets, where Schlichtholz (2019) later argued that the polar jet acts more prominently in this teleconnection pattern, bridging the NAO to the downstream Lake Baikal vortex. These existing studies on Rossby waves provide insights into possible pathways through which the NAO signals are propagated downstream, forming debates and inconsistencies on the relative importance of each pathway. The detailed mechanisms that cause NAO-linked anomalous temperatures in Asia, however, have not been explicitly addressed in current studies—such details could influence the interpretation of NAO-related anomalies, and are crucial in attributing the SAT teleconnection to the appropriate pathway(s). There therefore remains to be consensus on the teleconnection dynamics and pathways, and further studies are important for understanding climate variability and improving climate predictions.

Additionally, most of these existing studies focus only on reanalysis data. This approach provides only a short time sample, offering limited understanding of causality and the role of internal climate variability. For example, there is variability in how extended the NAO is Wang and Magnusdottir (2012), which could hinder a thorough understanding of the teleconnection dynamics given a short reanalysis dataset. In contrast, in large-ensemble climate models, inter-model differences in the NAO structure reflect jet variability (Parker *et al* 2019)—such differences, in addition to the generally much longer larger samples from model outputs, could provide insights into climatological factors that modulate the teleconnection.

By utilizing simulation outputs of from four large-ensemble coupled climate models, this study offers a novel and comprehensive perspective on the dynamics and pathways of the NAO downstream impact, which have not been extensively explored previously. We also quantify factors contributing to a strong teleconnection, and hence the predictability of downstream climate from the NAO. In particular, we hypothesize two chief factors that modulate the teleconnection strength: (i) the source amplitude (the local dominance of the NAO), and (ii) the pathways (the narrowness of the waveguides)—both of which are defined and reasoned in section 2.2. Together with the latest atmosphere reanalysis data, we quantify the relative importance of these two factors in modulating NAO downstream impacts on SAT variability in Eastern Eurasia.

2. Data and methodology

2.1. Data sources and preparation

With each providing at least 30 ensemble members, the four climate models used are: MIROC6, CNRM-CM6-1, NorCPM1, and CanESM5. MIROC6 is developed by the Japanese modeling community and has 50 ensemble members (Shiogama *et al* 2023). CNRM-CM6-1 is developed by Centre National de Recherches Météorologiques and CERFACS, featuring 30 ensemble members (Voldoire *et al* 2019). The NorCPM1 model, developed by the Norwegian Climate Prediction Model community, has 30 ensemble members (Bethke *et al* 2021). Finally, we use two ensembles of CanESM5, developed by the Canadian Centre for Climate Modelling and Analysis (CCCma) (Swart *et al* 2019) with alternative physics: 'p1' (40 members, uses conservative remapping for wind stress) and 'p2' (25 members, uses bilinear regridding). These total to four models, five ensembles of simulations. These models contribute to the Coupled Model Intercomparison Project Phase 6 (CMIP6), which compares and evaluates a number of state-of-the-art climate models globally. They generally perform well in simulating the NAO with respective strengths, including predictability for MIROC6 (Kataoka *et al* 2020), centres of action for CNRM-CM6-1 (Voldoire *et al* 2019), relevant modes of circulation patterns for CanESM5 (Swart *et al* 2019) and NorCPM1 (Bethke *et al* 2021), though common model biases exist and will be evaluated in section 4.

All data were taken from historical all-forcing runs, with monthly data spanning 1850–2014. Winter (DJF) data were extracted and used for calculations (the first seasonal mean is thus January 1851). In addition, monthly data between 1950 and 2014 was taken from the ERA5 reanalysis to provide observational inputs (Hersbach *et al* 2020), and have undergone the same seasonal averaging. The datasets used in this study have been regridded to a reduced resolution of $2.5° \times 2.5°$ for computational efficiency, which is appropriate for analyzing large-scale climate systems.

Variables directly obtained from the datasets include SAT, SLP, air temperature at higher levels, and geopotential height z. Wind is inferred from z using the geostrophic assumption:

$$u = -\frac{1}{f}\frac{\partial \Phi}{\partial y} = -\frac{1}{f}\frac{\cos\phi}{a}\frac{\partial \Phi}{\partial \phi}; \quad v = \frac{1}{f}\frac{\partial \Phi}{\partial x} = \frac{1}{f}\frac{1}{a}\frac{\partial \Phi}{\partial \lambda}; \quad \Phi = zg, \tag{1}$$

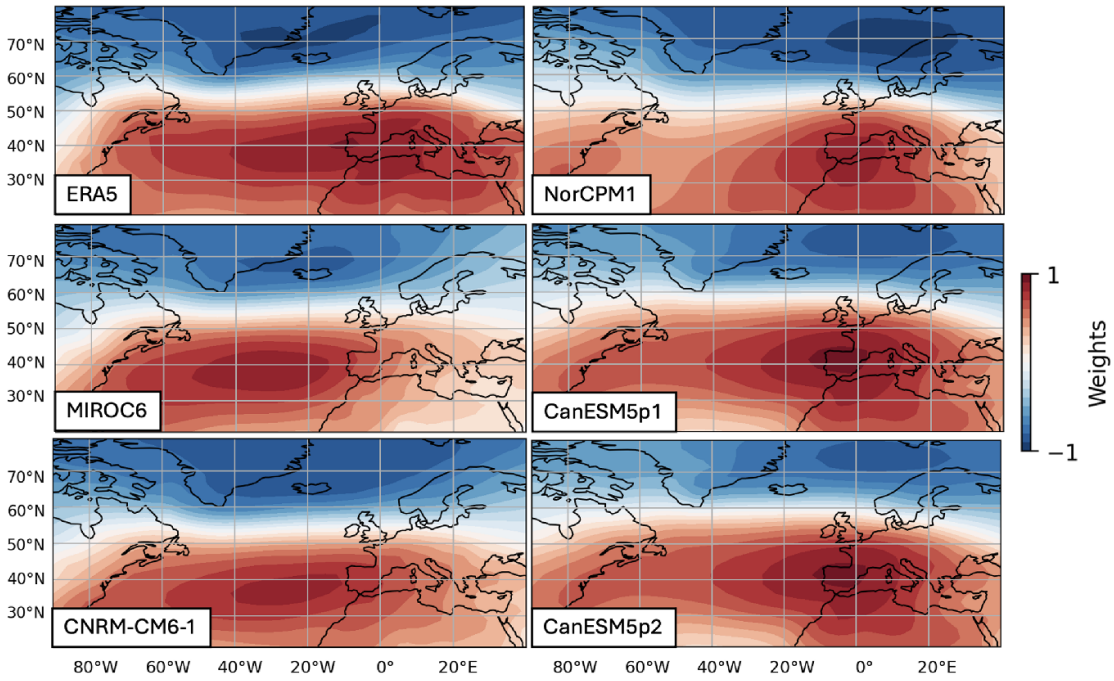

Figure 1. The mean leading EOF patterns of the North Atlantic SLP (i.e. the NAO pattern) in each model and ERA5.

where ϕ, λ, a, g are the latitude, longitude, the Earth radius and the gravitational acceleration respectively.

2.2. Defining the NAO index (NAOI)

Simple traditional definitions of the NAOI, such as station-based measurements and gridded SLP differences, may have limitations in capturing inter-model variability in the NAO pattern, so we adopt an empirical orthogonal function (EOF) definition (Wang *et al* 2014). The leading EOF of SLP over a large North Atlantic region is used ([90° W, 40° E] and [20° N, 80° N]), with the principal component timeseries yielding the NAOI. The mean leading EOF patterns in ERA5 and each model are shown in figure 1. This region is large enough such that in all models, the NAO dipole is well within the box, offering a measure of the NAO which allows for spatial variability across models. Using this definition, there is no notable long-term trend found in the NAOI over this period in the models. This stationarity allows analysis of the full model record and a fair comparison with reanalysis although the periods differ. The EOF definition gives rise to another parameter—the explained variance σ^2_{NAO} of the NAO pattern over the North Atlantic SLP. This will be used to measure the dominance (amplitude) of the NAO over other circulation patterns.

2.3. Teleconnection analysis

Maps of the temporal correlation between NAOI and SAT are used to present the teleconnection pattern in reanalysis and models. To examine the mechanisms of the teleconnection, we perform linear regression on NAOI of i) geopotential height at 300 hPa (z_{300}), used as an optimal pressure level at which to detect stationary Rossby wave propagation (Liu *et al* 2014), and ii) temperature advection at 850 hPa to measure the near-surface impacts (defined as $-\mathbf{u}\cdot\nabla T$, where $\mathbf{u}=(u,v)$ and T are the wind vector and air temperature).

Over all models, each ensemble member will be interpreted as a 164 year teleconnection time series. A collective analysis over all members gives insight into factors modulating this teleconnection. Each teleconnection time series has its own strength, R_{T}, defined as the Pearson correlation coefficient between the NAOI and an area-averaged SAT over a downstream area, identified in section 3.1. We hypothesize two modulating factors: the source (the NAO itself) and the pathways (stationary Rossby waveguides). If the NAO is more dominant over other local flows (shown by a higher EOF explained variance σ^2_{NAO}), it is reasonable to expect that it also exerts a stronger downstream control in that ensemble member.

On the other hand, as the Rossby waveguides mediate the waves that transport NAO signals downstream, their characteristics could also affect the teleconnection strength. These waveguides comprise strong vorticity gradients which trap Rossby waves, focusing and guiding them zonally over a long distance, facilitating teleconnections (Hoskins and Karoly 1981, Ambrizzi and Hoskins 1997). In the NAO teleconnection, the relevant waveguides are the subtropical and polar waveguides (Watanabe 2004,

Song *et al* 2014). Theoretically, when these jet streams and waveguides are narrower, they could restrict the dispersion of wave energy, preventing it from spreading meridionally (Wirth 2020). To test this in the NAO teleconnection context, we adopt the stationary Rossby wavenumber K_s (Hoskins and Karoly 1981):

$$K_s = \left(\frac{\beta_M \cos\phi}{\overline{u}}\right)^{\frac{1}{2}}; \quad \beta_M = \frac{2\Omega}{a}\cos^2\phi - \frac{\cos\phi}{a^2}\frac{\partial}{\partial\phi}\frac{1}{\cos\phi}\frac{\partial}{\partial\phi}(\overline{u}\cos\phi) \tag{2}$$

where β_M and Ω are the vorticity gradient parameter and the rotational angular speed of the Earth respectively. To measure the narrowness of a waveguide, we take $\overline{|\mathrm{d}K_s/\mathrm{d}y|}$: the average of the magnitude of the meridional derivative of K_s at 300 hPa over a waveguiding region (to be identified in section 3.3). The larger the derivative, the steeper the wavenumber drops from the central maximum K_s in a waveguide, indicating that it is narrower. There are locations where K_s is undefined since $K_s^2 < 0$. These are treated using a flexible derivative calculation—where there is a meridional boundary between defined and undefined K_s, forward/backward finite difference is used; otherwise central difference is used. Grid points with undefined K_s are discounted from the averaging. There are different methods to measure the narrowness of these pathways such as fitting a Gaussian function to a jet (Manola *et al* 2013, Wirth 2020); however on seasonal timescales, methods utilizing K_s work sufficiently well (Li *et al* 2020).

To understand what facilitates a strong teleconnection across all ensemble members, σ^2_{NAO} and $\overline{|\mathrm{d}K_s/\mathrm{d}y|}$ will be used as predictors for teleconnection strength R_T in a multiple linear regression model, i.e. ordinary least squares regression for:

$$R_T = \alpha\,\sigma^2_{\mathrm{NAO}} + \beta\,\overline{|\mathrm{d}K_s/\mathrm{d}y|} + \epsilon, \tag{3}$$

where α, β are fitted constants and ϵ is the residual term, alongside comparison to reanalysis results.

3. Results

3.1. Teleconnection pattern

Correlations between the NAOI and SAT are shown in figure 2, presenting the teleconnection patterns. In all model ensembles, a zonally extended positive teleconnection belt spans from the North Atlantic to the North Pacific, in a two-lobed structure similar to that previously found in reanalysis. It can be preliminarily observed that MIROC6 portrays the weakest teleconnection on average, while NorCPM1 portrays the strongest. A high-correlation region over Northeast Asia common to all models is indicated by the black boxes (enclosed by [75° E,125° E] and [50° N,75° N] and denoted NEA hereafter). This region is of high interest due to its long distance from the NAO source, as a representative example of the teleconnection control, and its position over the Siberian High system which has a strong influence over Asian climate (Zhou *et al* 2023). It is noteworthy that the correlation of the NAOI with temperature in this box is often comparable in magnitude to that over Northern Europe, much closer to the NAO itself. ERA5 exhibits a particularly strong and contiguous band of teleconnection compared to the models. The standard deviation of interannual winter SAT in this box across all model members is 2.6 K (2.2 K for ERA5), and using linear regression the NAO drives 1.9 ± 0.3 K per unit NAOI on average in this region (1.6 K/NAOI for ERA5).

3.2. Pathways and dynamics

To understand atmospheric circulation structures linked to the NAO teleconnections, we computed the regressions of z_{300} onto the NAOI. The NAOI-z_{300} regression maps are shown in figure 3. All models show an NAO-controlled anticyclonic circulation anomaly over Northeast Asia, consistent with reanalysis. MIROC6 has a notably less significant anomaly and CNRM-CM6-1 has an eastward-shifted anomaly, which could be related to their weaker teleconnections on average. Previous studies based on reanalysis suggested that a similar anomaly (discovered through regressing against storm activity) is excited mainly by wavenumber-3 Rossby waves guided by the polar jet (Schlichtholz 2018, 2019), but some highlighted that the subtropical (Asian) jet is key to enhancing the NAO downstream control (Branstator 2002, Watanabe 2004).

The regression results here could provide reconciling insights for these views, as the geopotential height anomaly over Northeast Asia is typically elongated southeast-wards, spanning regions which are influenced by the polar and subtropical jets. Although the NEA anticyclone is primarily under the polar jet, it is close to the junction where both streams of waves meet (as supported by WAF diagrams in Song *et al* 2014), so its phase and amplitude could be modulated by signals from both streams. This suggests the potential importance of *both* pathways in forming the teleconnection, with their interaction producing a highly efficient channel for the NAO to influence climate over Asia and beyond.

With the improved understanding of Rossby wave propagation pathways, the role of heat advection in this teleconnection can be analyzed further. The NAOI-advection at 850 hPa regression maps are shown in figure 4. Reanalysis and all models present two patches of anomalous warm advection—one over Northern Europe and another over Northeast Asia: during NAO+ these regions are heated anomalously

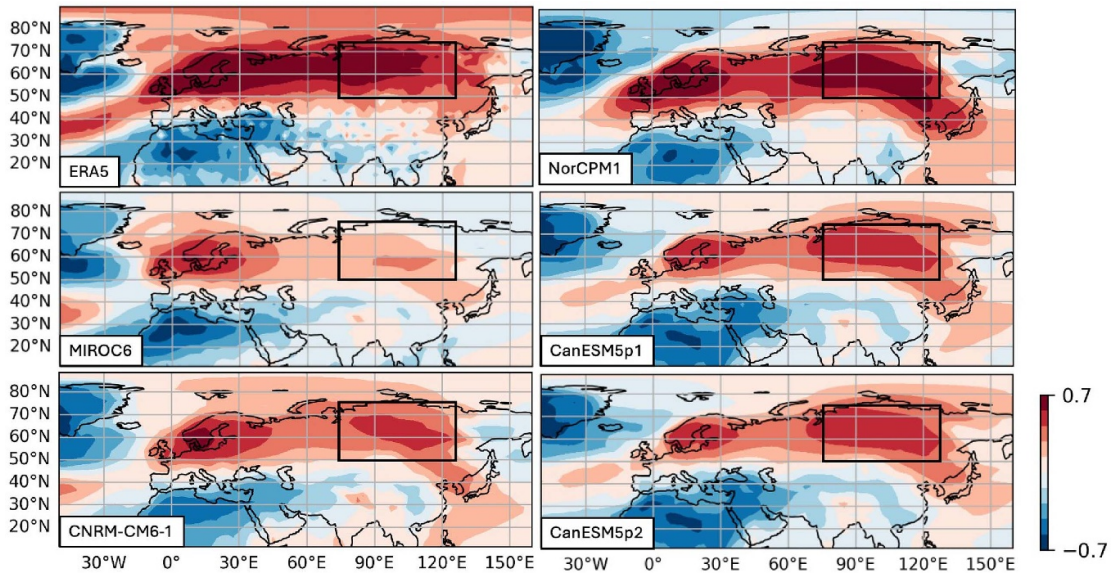

Figure 2. Correlation of SAT at each grid point with the NAOI from ERA5 reanalysis (1951–2014) and the five model ensembles (as mean correlations over each ensemble) (1851–2014). The color bar is saturated over the specified limits. The boxes define the common key region 'NEA'.

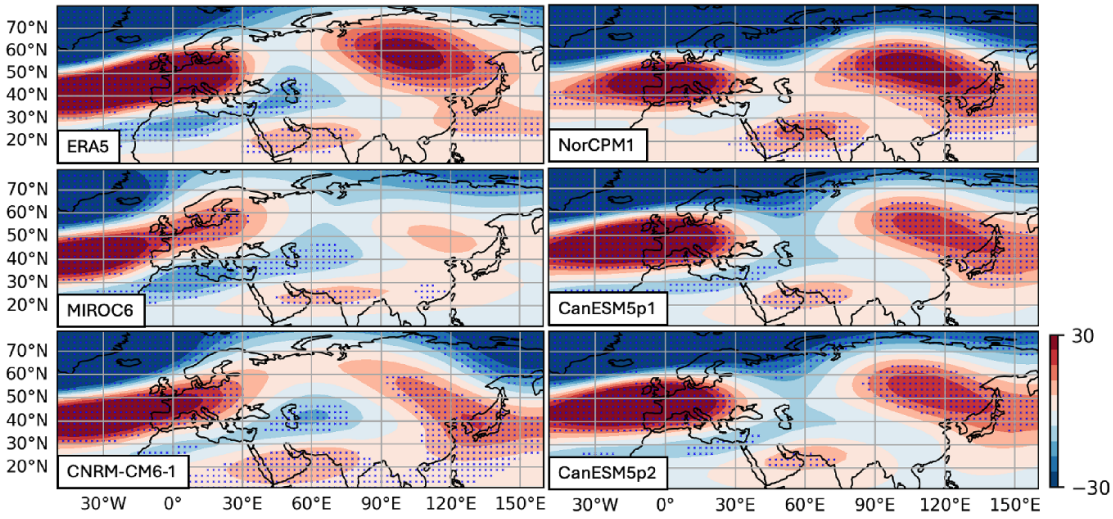

Figure 3. NAOI-z_{300} regression maps from the ERA5 reanalysis (1951–2014) and the five model ensembles (as mean regression over each ensemble) (1851–2014). The color bar is in km, saturated over the specified limits. Dotted areas are where the regression is significant within a 95% confidence interval on average.

by horizontal advection, and conversely cooled during NAO–. This advection pattern is much less continuous than the SAT correlation map in figure 2, with notable resurgences in amplitude near the Pacific coastline.

The presence of warm advective tendencies all across northern Eurasia, aligned with the polar jet stream, suggests there is some transport of warm air eastward from the vicinity of the Nordic Seas. However, advection is considerably amplified over the Pacific onshore wind portion in the anomalous high-level circulation (from the circulation in figure 3). The vertical structure of this pressure anomaly is coherently connected (Schlichtholz 2019), so that the upper-level Rossby waves are linked to the low-level atmospheric circulation, which plays an important role in local heat advection. This overlap between advection and the onshore-wind portion of the NEA anticyclone suggests that during NAO+, the NAO-controlled NEA anticyclone advects warm air from the Pacific (see positive anomalies extending northwestward from the vicinity of Japan to NEA), bringing a warming effect to Asia, and vice versa during NAO–. Again, MIROC6 (which

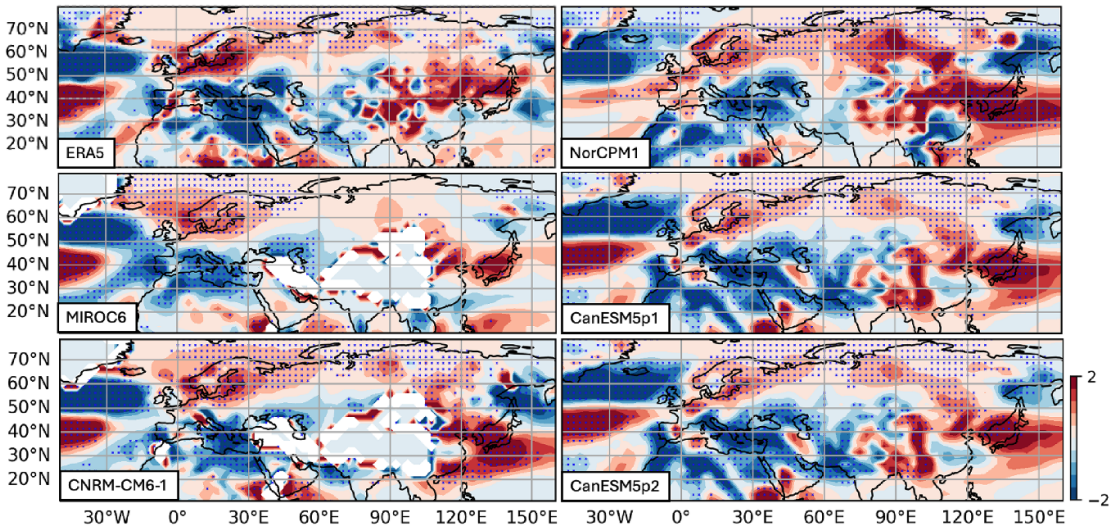

Figure 4. NAOI-advection at 850 hPa regression map from the ERA5 reanalysis (1951–2014) and the five model ensembles (as mean regression over each model) (1851–2014). The color bar is in 10^{-6} Ks^{-1}, saturated over the specified limits. White patches indicate absence of data due to high terrain. Dotted areas are where the regression is significant within a 95% confidence interval on average.

has the weakest teleconnection) presents the weakest anomalous onshore advection over the region, further supporting its relevance to the teleconnection. Xie *et al* (1999) reported the possible role of anomalous advection from upstream; however, results here combining reanalysis and model outputs suggest a greater importance of advection from the Pacific Ocean. While a band of weak but positive temperature advection can be seen following the westerlies across the continent in all the datasets in figure 3, there is a stronger local effect which dominates over NEA, as a consequence of advection from the Pacific. Altogether, these complement the planetary scale Rossby waves over both the polar and subtropical pathways in inducing the NAO downstream temperature influence.

3.3. Mean-state modulation: model and ensemble variability

Over the four models, there are 175 ensemble members, each with a unique measured teleconnection. This section explores how the teleconnection strength is affected by mean-state factors from the source and the pathways: the NAO local dominance (σ^2_{NAO}) and narrowness of waveguides $\overline{|\mathrm{d}K_s/\mathrm{d}y|}$. In section 3.1, a key NAO-controlled region NEA was defined. In this section, the teleconnection strength R_T is defined as the Pearson correlation coefficient between the NAOI and the average SAT over NEA in an ensemble member. On average over each ensemble, R_T is highly stationary over time, suggesting that external forcing minimally affects this teleconnection. Over all members, R_T is regressed onto σ^2_{NAO} and $\overline{|\mathrm{d}K_s/\mathrm{d}y|}$ to understand the contribution of these factors.

To justify the use of the waveguide narrowness further, the mean of the ensemble K_s in each model (and from ERA5) is shown in figure 5(a). In all panels, two zonal waveguides can be identified: the polar waveguide between 40° N and 60° N, and the subtropical waveguide between 10° N and 30° N. Sections of these converge near southern Japan as mentioned in section 3.2. However, the widths and separation of the waveguides varies across models. From the model plots, NorCPM1 has the most stratified and narrow waveguides, while MIROC6 has the least. For comparison, the mean teleconnection strength R_T in these ensembles are 0.261 (MIROC6), 0.497 (CNRM-CM6-1), 0.735 (NorCPM1), 0.484 (CanESM5p1), 0.494 (CanESM5p2). This comparison suggests that the more stratified and narrowed the waveguides, the stronger the teleconnection. To quantitatively understand the influence of the waveguide width, the magnitude of meridional derivative is used, averaged over a waveguiding area (defined as 'WR', shown in figure 5(a)) enclosed by [0° E, 120° E] and [5° N, 70° N]. This area is optimized to regression performance and physical interpretation. Figure 5(b) is an example of $\overline{|\mathrm{d}K_s/\mathrm{d}y|}$ in ERA5, showing that this quantity correctly rewards steep waveguide boundaries in narrower waveguides. As discussed later, ERA5 has a relatively high $R_T = 0.713$ even though its waveguides are most similar to those of MIROC6 (though slightly more separated) in which the teleconnection is significantly stronger.

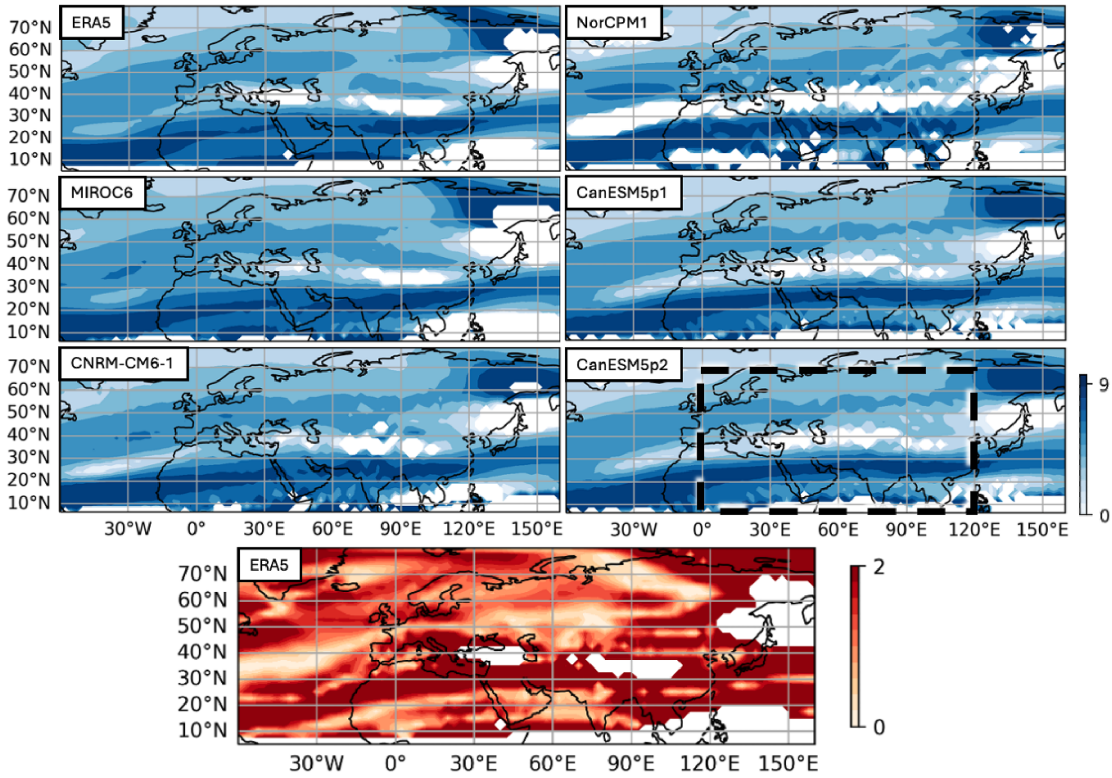

Figure 5. (a) Stationary wavenumber K_s, in units of (Earth radius)$^{-1}$, from ERA5 reanalysis (1951–2014) and ensemble means from each model (1851–2014). The black and white arrows in the ERA5 panel indicate the rough locations of the polar and subtropical waveguides respectively. The box in the CanESM5p2 panel denotes the waveguiding region 'WR'. (b) Example $\overline{|\mathrm{d}K_s/\mathrm{d}y|}$ from the ERA5 reanalysis, in units of 10^{-6} (Earth radius)$^{-1}$ m^{-1}. Values exceeding the upper limit of the color bars appear saturated.

Therefore, other factors are likely to play a role in modulating the teleconnection as well.

Multiple linear regression results between R_T and σ^2_{NAO}, $\overline{|\mathrm{d}K_s/\mathrm{d}y|}$ are shown in figure 6 and table 1. Regression is performed on 1851–2014 for models, but for direct comparison with ERA5 this is also repeated for 1951–2014. Correlation statistics for 1851–1950 are additionally shown in the table for reference.

From the scatter plots in figure 6(a), there is a positive correlation between R_{T} and each of the two factors (σ^2_{NAO} and $\overline{|\mathrm{d}K_s/\mathrm{d}y|}$). The contribution of inter-model and intra-model variabilities are comparable, although some model clustering is observed. From table 1, the two factors are only very weakly correlated with each other in both periods, demonstrating that they are suitable predictors for a multiple linear regression model. In the model period, the two factors combine to explain a robust 70% of the teleconnection strength variability, where each factor contributes approximately equally[1]. In the reanalysis period (1951–2014) and prior (1851–1950), the R^2 values are similar, suggesting that in addition to the aforementioned stationarity in teleconnection strength (R_{T}) itself, the modulation from the two factors also remains stationary over time. (The weaker correlations compared to the model period (1851–2014) are likely due to shorter datasets).

It is interesting to examine whether this model-based relationship is consistent with the ERA5 reanalysis. Standardized residuals σ measure the extent a data point diverges from a regression model. For the reanalysis period, the ERA5 is $1.9-\sigma$ away from the model, which shows only marginally consistent relationships between the two factors and R_{T}. From figure 6(b), ERA5 appears on the edge of the relationship between the observed and the expected R_{T} from the multiple regression, but not as an outlier. Considering the two predictors separately, the reanalysis shows a strong R_{T} and is within the model spread in terms of how σ^2_{NAO} contributes to this. However, this large R_{T} value is inconsistent with the model spread in $\overline{|\mathrm{d}K_s/\mathrm{d}y|}$, suggesting that some models might be achieving a strong teleconnection by overestimating the strength of the waveguides.

[1] Supplementary regressions over models are conducted between R_{T} and $\overline{|\mathrm{d}K_s/\mathrm{d}y|}$ over the polar and subtropical waveguides *separately* (within the same 'WR' box in figure 5(a), but divided along 40° N. The R^2 values are 0.45 and 0.67 respectively, suggesting the subtropical waveguide narrowness is relatively more important.

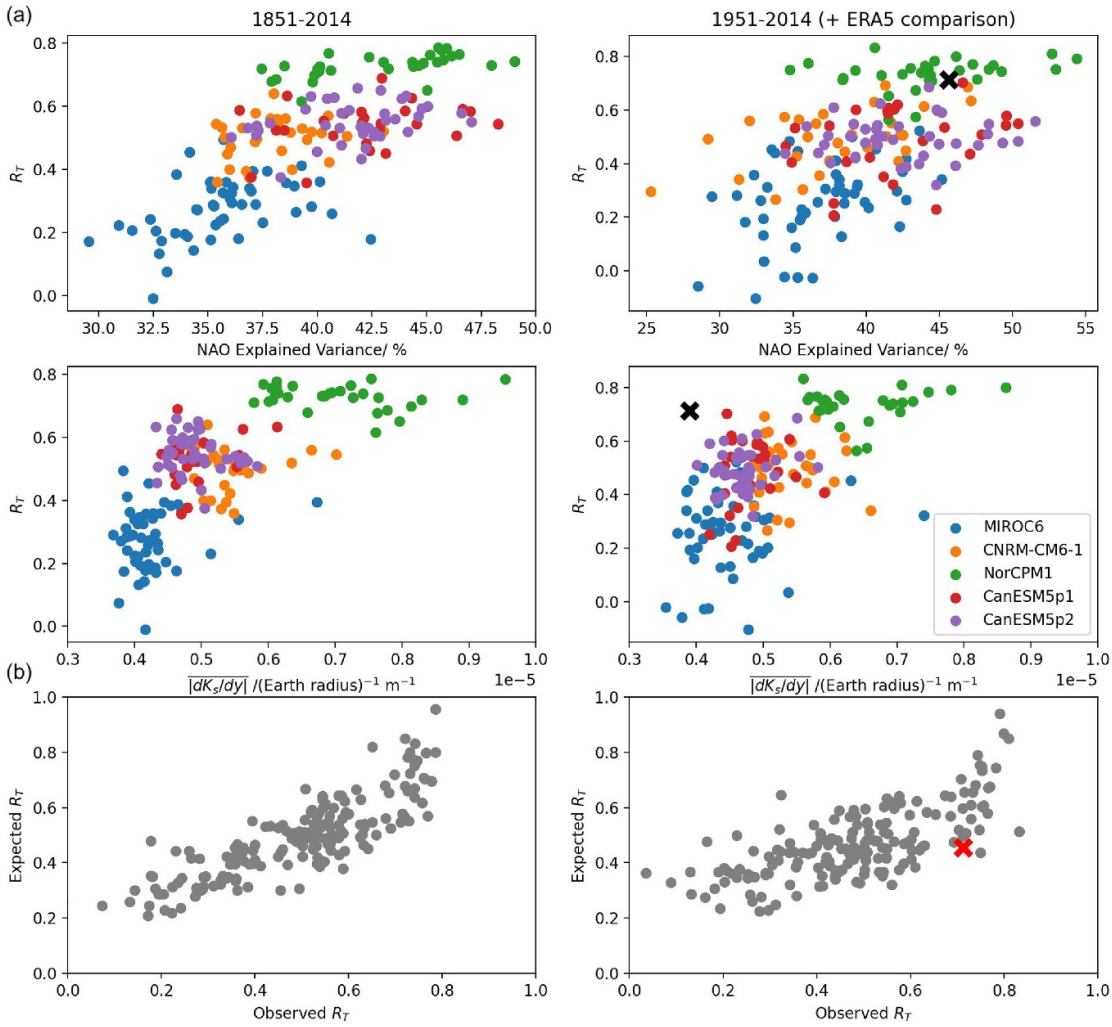

Figure 6. Multiple linear regression results. (a) Scatter plots of R_T versus σ^2_{NAO} and $\overline{|dK_s/dy|}$, in the model period 1851–2014 and the ERA5 period 1951–2014. In plots for the latter period, a cross marks the ERA5 value. (b) Expected R_T using the constructed multiple linear regression model versus the observed over all ensembles for each period; for 1951–2014 a cross marks the ERA5 value.

Table 1. Multiple linear regression statistics: teleconnection strength (R_T) with two predictors (σ^2_{NAO} and $\overline{|dK_s/dy|}$). R^2_{full} is the correlation coefficient of the regression model using both predictors; R^2_{cross} is that between the two predictors; $R^2_{\overline{|dK_s/dy|}}$ is that between R_T and $\overline{|dK_s/dy|}$, while $R^2_{\sigma^2_{NAO}}$ is that between R_T and σ^2_{NAO}.

Period	R^2_{full}	R^2_{cross}	$R^2_{\overline{\lvert dK_s/dy\rvert}}$	$R^2_{\sigma^2_{NAO}}$
1851–2014	0.70	0.18	0.51	0.48
1851–1950	0.58	0.07	0.28	0.44
1951–2014	0.52	0.03	0.30	0.31

4. Discussions and conclusion

The inclusion of ensemble model data has enabled improved sampling of previously known mechanisms, and further evidence of the causality in the teleconnection. Results from this study could help to reconcile theories of this teleconnection—whether it is mediated by continuous advection, Rossby waves along the subtropical jet, the polar jet, or both. Both reanalysis and model data demonstrate that the teleconnection originates not simply from a continuous advection belt from upstream across Eurasia, but in addition with a strong contribution from stationary Rossby waves along both the polar and the subtropical waveguides. These waves directly drive downstream local advection that plays an acute role in facilitating anomalous heating or cooling, for example by bringing warm air from the Pacific Ocean onshore. This emphasizes the role of large-scale Rossby waves acting to transport signals from one point on Earth to another remote location. The fact that both pathways matter suggests that the waves do interact, and it is impractical to take an isolated view of any single pathway. This highlights the relevance of wave dynamics

(e.g. reflection, interference) when developing theories for teleconnections as such.

This study also demonstrated that internal climate variability modulates the strength of the teleconnection even in very long data samples, an underappreciated factor as past studies relied solely on reanalysis. Model ensemble members with a locally dominant NAO tend to produce stronger downstream teleconnection, as might be expected. The narrowness of mean-state waveguides has also been shown to have an impact: if the waveguides are narrower, the teleconnection strength tends to increase. This confirms the importance of the waveguiding mechanism: as waves get refracted towards a high-K_s belt, they preferentially travel along this waveguide. Narrower waveguides prevent waves from escaping, forming more efficient teleconnection channels. These two factors combine roughly equally to explain up to 70% of the variance in teleconnection strength across ensemble members, proving the importance of these modulating mean-state variables.

In real-world application, the waveguide characteristics and NAO dominance could change over longer timescales. For example, studies have shown that the NAO variability could differ between decades (Hanna *et al* 2015). These could cause variations in the teleconnection strength over time, and in turn the weight of the NAOI in downstream climate predictions. Therefore, when incorporating the NAO as a predictor for Eurasian climate, it is important to monitor these modulating factors and their influence on climate predictability.

Discrepancies between reanalysis and model data suggest that there are model limitations as ERA5 is only marginally consistent with the multiple linear regression. Specifically, the ERA5 teleconnection strength is higher than predicted by the models for an equivalent σ^2_{NAO}; it has waveguides that are less narrow (and more smoothly blended, as seen from figure 5) than most model ensemble members. Other studies have revealed some systematic biases in climate models, for example underestimating the multidecadal NAO variability (Bracegirdle 2022), and common jet biases which could lead to mis-characterization of the waveguiding effect (Pithan *et al* 2016). This suggests that while some models have a realistic strength of the downstream teleconnection, this may not reflect the correct balance in the underlying mechanisms. It is also interesting that members of the same models cluster in some plots in figure 6, highlighting important inter-model differences in the simulated NAO. Correcting these model biases is necessary for obtaining a more thorough understanding of the NAO downstream influence that agrees with historical observations.

Although not presented, it is worth noting that in some models (and ERA5), there is a notable phase-asymmetry, with the strength of the downstream control differing between NAO+ and NAO–. However, this is not consistent across all models and should be a topic for future investigation. The influence of the NAO over downstream precipitation could be another extension, which could help construct a more complete picture of the complex mechanisms that bring climate signals downstream to Eurasia.

Finally, the analysis on dynamics in this study relied on the stationarity of the model teleconnections. There remains a need to address model limitations, including some climate models not responding well to external forcing and underestimating NAO trends (Scaife and Smith 2018, Blackport and Fyfe 2022). This study adopted a linear regression approach to provide an overview of the teleconnection. In reality, non-linearities exist, as intermediate factors (e.g. jet position, storm activity) vary with NAO polarity. Combining these considerations with machine learning approaches over more large-ensemble climate datasets could further improve downstream climate prediction using the NAO as a skillful predictor.

Data availability statement

All data that support the findings of this study are included within the article (and any supplementary files).

Acknowledgments

K Y acknowledges support by the UKRI Horizon Europe Guarantee MSCA Postdoctoral Fellowship EP/Y029119/1, and by the John Fell Fund financed by Oxford University Press (Project Reference: 0013106). TW was supported by NERC grants NE/T013451/1 and NE/W005875/1. This research was funded in whole, or in part, by the UKRI [EP/Y029119/1]. The contents reflect only the author's views and not the views of the UKRI. For the purpose of Open Access, the author has applied a CC BY public copyright licence to any Author Accepted Manuscript version arising from this submission.

References

Ambrizzi T and Hoskins B J 1997 Stationary Rossby-wave propagation in a baroclinic atmosphere *Q. J. R. Meteorol. Soc.* **123** 919–28

Baker L H, Shaffrey L C, Johnson S J and Weisheimer A 2024 Understanding the intermittency of the wintertime North Atlantic Oscillation and East Atlantic Pattern seasonal forecast skill in the Copernicus C3S multi-model ensemble *Geophys. Res. Lett.* **51** e2024GL108472

Bethke I *et al* 2021 NorCPM1 and its contribution to CMIP6 DCPP *Geosci. Model Dev.* **14** 7073–116

Blackport R and Fyfe J C 2022 Climate models fail to capture strengthening wintertime North Atlantic jet and impacts on Europe *Sci. Adv.* **8** eabn3112

Bracegirdle T J 2022 Early-to-Late winter 20th century North Atlantic multidecadal atmospheric variability in observations, CMIP5 and CMIP6 *Geophys. Res. Lett.* **49** e2022GL098212

Branstator G 2002 Circumglobal teleconnections, the jet stream waveguide and the North Atlantic Oscillation *J. Clim.* **15** 1893–910

Hanna E, Cropper T E, Jones P D, Scaife A A and Allan R 2015 Recent seasonal asymmetric changes in the NAO (a marked summer decline and increased winter variability) and associated changes in the AO and greenland blocking index *Int. J. Climatol.* **35** 2540–54

Hersbach H *et al* 2020 The ERA5 global reanalysis *Q. J. R. Meteorol. Soc.* **146** 1999–2049

Hoskins B J and Karoly D J 1981 The steady linear response of a spherical atmosphere to thermal and orographic forcing *J. Atmos. Sci.* **38** 1179–96

Hurrell J W 1996 Influence of variations in extratropical wintertime teleconnections on Northern Hemisphere temperature *Geophys. Res. Lett.* **23** 665–8

Hurrell J W and Van Loon H 1997 Decadal variations in climate associated with the North Atlantic Oscillation *Clim. Change* **36** 301–26

Kataoka T, Tatebe H, Koyama H, Mochizuki T, Ogochi K, Naoe H, Imada Y, Shiogama H, Kimoto M and Watanabe M 2020 Seasonal to decadal predictions with MIROC6: description and basic evaluation *J. Adv. Model. Earth Syst.* **12** e2019MS002035

Lee J, Sperber K R, Gleckler P J, Taylor K E and Bonfils C J 2021 Benchmarking performance changes in the simulation of extratropical modes of variability across CMIP generations *J. Clim.* **34** 6945–69

Li R K K, Woollings T, O'Reilly C and Scaife A A 2020 Tropical atmospheric drivers of wintertime European precipitation events *Q. J. R. Meteorol. Soc.* **146** 780–94

Liu Y, Wang L, Zhou W and Chen W 2014 Three Eurasian teleconnection patterns: spatial structures, temporal variability and associated winter climate anomalies *Clim. Dyn.* **42** 2817–39

Luo D, Yao Y, Dai A and Feldstein S B 2015 The positive North Atlantic Oscillation with downstream blocking and Middle East snowstorms: the large-scale environment *J. Clim.* **28** 6398–418

Manola I, Selten F, de Vries H and Hazeleger W 2013 "Waveguidability" of idealized jets *J. Geophys. Res.: Atmos.* **118** 10432–40

Parker T, Woollings T, Weisheimer A, O'Reilly C, Baker L and Shaffrey L 2019 Seasonal predictability of the winter North Atlantic Oscillation from a jet stream perspective *Geophys. Res. Lett.* **46** 10159–67

Pithan F, Shepherd T G, Zappa G and Sandu I 2016 Climate model biases in jet streams, blocking and storm tracks resulting from missing orographic drag *Geophys. Res. Lett.* **43** 7231–40

Scaife A A and Smith D 2018 A signal-to-noise paradox in climate science *npj Clim. Atmos. Sci.* **1** 28

Schlichtholz P 2018 Climate impacts and arctic precursors of changing storm track activity in the Atlantic-Eurasian region *Sci. Rep.* **8** 17786

Schlichtholz P 2019 Upper-tropospheric bridging of wintertime surface climate variability in the Euro-Atlantic region and northern Asia *Sci. Rep.* **9** 14660

Shiogama H, Tatebe H, Hayashi M, Abe M, Arai M, Koyama H, Imada Y, Kosaka Y, Ogura T and Watanabe M 2023 MIROC6 large ensemble (MIROC6-LE): experimental design and initial analyses *Earth Syst. Dyn. Discuss.* **2023** 1–28

Song J, Li C and Zhou W 2014 High and low latitude types of the downstream influences of the North Atlantic Oscillation *Clim. Dyn.* **42** 1097–111

Swart N C *et al* 2019 The Canadian earth system model version 5 (CanESM5. 0.3) *Geosci. Model Dev.* **12** 4823–73

Voldoire A *et al* 2019 Evaluation of CMIP6 deck experiments with CNRM-CM6-1 *J. Adv. Model. Earth Syst.* **11** 2177–213

Wang Y-H and Magnusdottir G 2012 The shift of the northern node of the NAO and cyclonic Rossby wave breaking *J. Clim.* **25** 7973–82

Wang Y-H, Magnusdottir G, Stern H, Tian X and Yu Y 2014 Uncertainty estimates of the EOF-derived North Atlantic Oscillation *J. Clim.* **27** 1290–301

Watanabe M 2004 Asian jet waveguide and a downstream extension of the North Atlantic Oscillation *J. Clim.* **17** 4674–91

Wirth V 2020 Waveguidability of idealized midlatitude jets and the limitations of ray tracing theory *Weather Clim. Dyn.* **1** 111–25

Xie S-P, Noguchi H and Matsumura S 1999 A hemispheric-scale quasi-decadal oscillation and its signature in northern Japan *J. Meteorol. Soc. Japan II* **77** 573–82

Ye K, Messori G, Chen D and Woollings T 2022 An NAO-dominated mode of atmospheric circulation drives large decadal changes in wintertime surface climate and snow mass over Eurasia *Environ. Res. Lett.* **17** 044025

Zhou F, Shi J, Liu M H and Ren H C 2023 Linkage between the NAO and Siberian high events on the intraseasonal timescale *Atmos. Res.* **281** 106478